JOURNAL OF MATERIALS SCIENCE 31 (1996) 2487–2493

The influence of molecular weight and mould temperature on the skin–core morphology in injection-moulded polypropylene parts containing weld lines

W. WENIG, C. STOLZENBERGER
Applied Physics Laboratory, University of Duisburg, 47048 Duisburg, Germany

The sandwich structure of injection-moulded polypropylene parts with and without weld lines has been investigated using optical microscopy, X-ray scattering, and differential scanning calorimetry. It was found that the skin-layer thickness is strongly dependent on whether the mould is injected through one gate or through two gates. Samples containing a weld line show a much lower skin-layer thickness than samples without a weld line. This difference, however, depends strongly on the molecular weight of the polypropylene. The skin-layer thickness also varies along the flow path and decreases with increasing mould temperature. While most of the polypropylene crystallizes in the crystallographic α-modification, in the textured skin layer, some β-modification occurs. The β-crystallinity depends on the molecular weight but disappears in the weld line. X-ray investigations exhibited a bimodal crystal orientation in the skin layer, one with the *c*-axis oriented parallel to the flow direction, the second one with the *a**-axis oriented parallel to the flow direction. The core exhibited only a weak *c*-axis orientation. In the skin, the metastable α_1-modification was found.

1. Introduction

It is well established that injection-moulded polypropylene parts exhibit a sandwich structure which develops as a result of the cooling conditions during injection of the (hot) melt into the (cold) mould [1–5]. This structure can be roughly separated into three layers [1, 2]: a "structureless" skin, a spherulitic core, and an oriented transition zone between skin and core. A closer look at the morphology reveals [2], that the skin consists of several morphologically different layers. The thickness of each layer is controlled by the shear conditions during injection of the melt and is therefore dependent on the processing conditions. Janeschitz-Kriegl [6, 7] showed, that the sandwich structure can be approximately calculated. The most important parameters are the temperature of the melt, the velocity of the melt front and the molecular weight distribution.

An even more complicated structure occurs when in the mould the melt is directed such that two or more fronts meet (e.g. recombining of the melt after flowing round an obstacle) or when the melt is injected into the mould through separate gates. In both cases a welding seam is formed. Fisa [8] showed by investigating the orientation of inorganic fillers, that the method of impinging affects the orientation of the melt. Weld lines generally affect the mechanical properties of moulded parts by lowering their tensile properties. Piccarolo *et al.* [9, 10] found notches at the sites of the weld lines whose sizes were dependent on the processing parameters. Trotignon *et al.* [4] investigated the crystal morphology (α- and β-modifications). Correlations between the processing parameters and the composition of the crystal modifications were found. Electron microscopy studies [11] showed that, in the weld line, the content of the β-modification is generally lower than elsewhere in the sample [12].

In this work, we investigated the morphology and the crystal structure of injection-moulded polypropylene parts, employing optical microscopy and small- (SAXS) and wide-angle X-ray scattering (WAXS).

2. Experimental procedure

2.1. Sample preparation

Isotactic polypropylene with molecular weights $M_w = 243\,000$ (low molecular weight samples) and $M_w = 753\,000$ (high molecular weight samples) was used to produce injection-moulded standard tensile bars according to DIN 53455 (length = 150 mm, thickness = 3 mm) by injecting through one gate or two gates, respectively. The temperature of the melt was 240 °C and two sets of samples for each molecular weight were prepared using the mould temperatures $T_w = 40$ and 100 °C. The processing parameters were as follows: form filling pressure $p_e = (3 \times 10^7 \pm 5 \times 10^5)$ Pa; mould-filling time $t_f = 270$ ms; holding time $t_e = 4.0$ s; holding pressure $p_h = (6 \times 10^6 \pm 5 \times 10^5)$ Pa.

0022–2461

To investigate morphological changes as a function of location, segments were cut out from the bars: one segment was taken from the centre (segment 2), the other two from both ends of the bar at a distance of 27.5 mm from the centre (Fig. 1). From each segment, five microtomed sections with thicknesses of ~ 20 μm were made (Fig. 2) and the skin and core pieces were used for the X-ray measurements.

2.2. Microscopy

For observation in the optical microscope (Leitz Metallux II), the microtomed sections were placed between microscope slides. Crossed polarizers were used and the microscope image was both monitored on a video screen and photographed with $\times 200$ magnification. At this magnification, the micrographs showed a sample segment of 200 μm $\times$ 500 μm.

2.3. X-ray experiments

Small-angle X-ray scattering curves were recorded using a Kratky compact camera. The setting of the camera was such that sufficiently high resolution was ensured (entrance slit width = 30 mm, detector slit width = 75 mm, distance sample–detector slit = 22 cm).

The measurements were controlled by a computer and the temperature of the cooling water was kept constant through a constant-temperature unit. CuK_α radiation was used and monochromatization was achieved by using a nickel filter in conjunction with pulse-height analysis.

Each curve was recorded several times in an angular range corresponding to 0.7×10^{-4} nm $\leqslant s \leqslant$ $40\,10^{-4}$ nm ($s = 2\sin\theta/\lambda$, 2θ being the scattering angle and λ the X-ray wavelength).

Flat camera exposures were taken using a Philips PW 1012/90 camera. To determine the distance sample to film, A, a KCl powder sample was used. For a known spacing d_{hkl}, A is yielded from the equation $2\theta = \arctan(D/2A)$; $d_{hkl} = \lambda/2\sin(\theta)$ where D is the reflection diameter. For all calculations, the following unit cell parameters were employed [13, 14]: α-modification: $a = 0.663$ nm, $b = 0.2078$ nm, $c = 0.650$ nm, $\beta = 99\,°5'$, β-modification: $a = 0.1908$ nm, $c = 0.649$ nm.

Wide-angle X-ray scattering curves were measured using a Philips PW 1380 Goniometer.

CuK_α radiation was used and monochromatization was achieved using a graphite monochromator. To determine the "order-parameter", the composition of α_1 and α_2 monoclinic crystal modifications, the angular range $32° \leqslant 2\theta \leqslant 44°$ was measured separately at higher resolution.

2.4. Calorimetric measurements

Differential scanning calorimetry (DSC) curves were recorded using a Netzsch heat-flux DSC 444 calorimeter. All samples were heated from 20–220 °C with a heating rate of 10 K min^{-1} in a nitrogen atmosphere. A second sample was run using identical conditions.

2.5. Tensile tests

Mechanical tests were performed using a Roell and Korthaus testing machine. Stress–strain curves were recorded automatically. Each experiment was repeated five times, both applying stress- and strain-controlled forces. The strain rate amounted to $\dot{\varepsilon} = 10^{-3}$ s^{-1}.

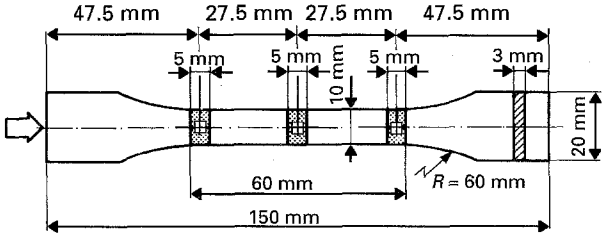

Figure 1 Dimensions of standard tensile test bar and position of segments cut out of the bar.

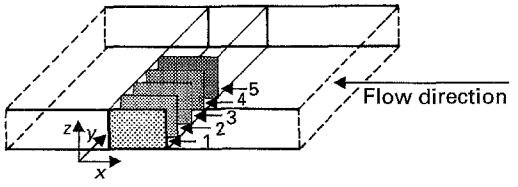

(a)

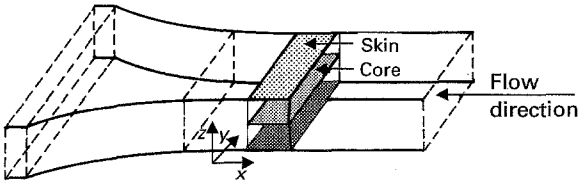

(b)

Figure 2 Positions of samples cut out from the standard tensile bars for (a) optical and (b) X-ray and calorimetric investigations.

3. Results and discussion

The polarization micrographs of all microtomed sections display a sandwich structure (see Fig. 3). Three zones can be distinguished. Zone I, the skin, seems to be without any structure, but several investigations show that it contains either a microspherulitic morphology [15] or a highly oriented fibrillar structure [16]. Zone II is the oriented "transition zone", which can be separated into three subzones. The third zone, zone III (core), shows a spherulitic structure with spherulites up to 120 μm diameter. Zone II is divided into a microspherulitic zone IIa, a textured zone IIb and a zone IIc exhibiting transcrystallization with the growth direction perpendicular to the flow direction in this zone. Zones I to IIc are commonly called the skin layer.

Table I gives the thicknesses of the skin layer for the investigated sample segments. In all samples without a weld line the skin layer is thicker than in samples containing a weld line. Here the thicknesses decrease

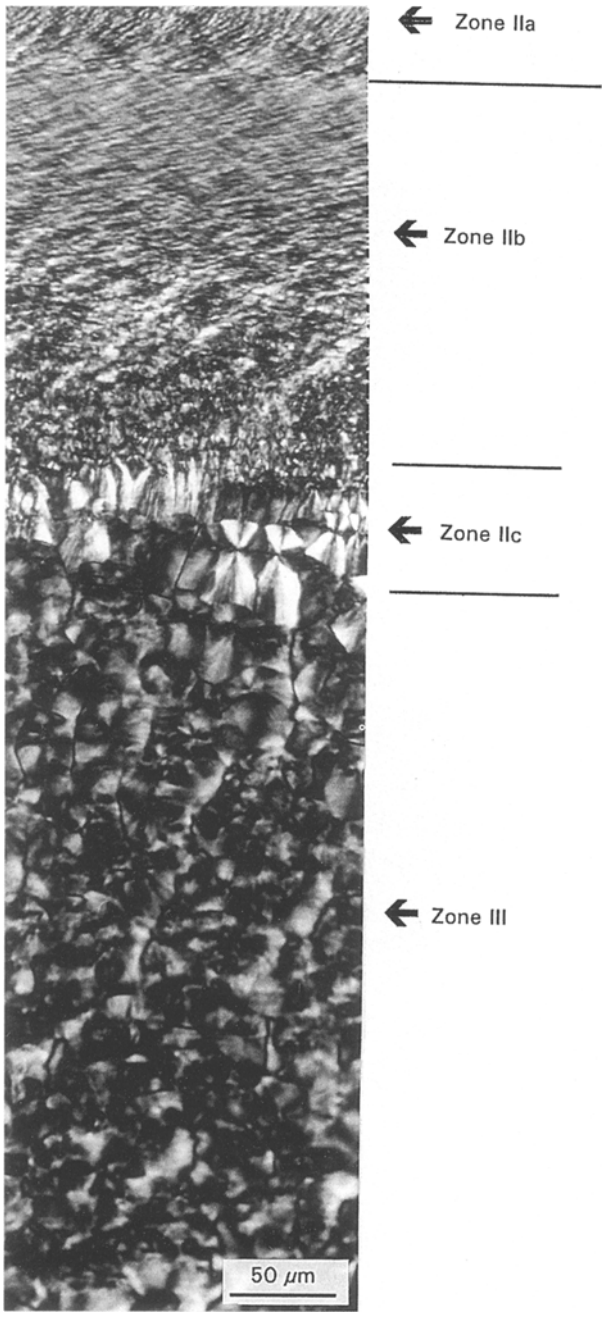

Figure 3 Polarization micrograph of the skin–core morphology (low molecular weight sample, $T_w = 40\,°C$, segment 1).

TABLE I Skin-layer thicknesses

Segment	Skin-layer thickness (μm) T_w without weld line		T_w with weld line	
	40 °C	100 °C	40 °C	100 °C
Low molecular weight samples				
1	201	186	15	15
2	175	175	5	2.5
3	153	158	15	15
High molecular weight samples				
1	258	226	334	294
2	249	211	33	6
3	224	188	313	273

nearly linearly with distance from the gate, while for the samples with a weld line the thickness is identical for sample segments 1 and 3 and lower for segment 2 (containing the weld line). The mould temperature influences the skin-layer, especially in the high molecular weight samples: for $T_w = 100\,°C$ the thickness is lower than for $T_w = 40\,°C$. Generally, the high molecular weight samples show a thicker skin layer than the low molecular weight samples. The spherulites are all of type I (α-modification, positive birefingence) and type III (β-modification, negative birefringence). Type I appears in all layers, while type III can be detected only in zone IIc. No β-form spherulites appear in the low molecular weight samples with weld line at $T_w = 40\,°C$ and in the high molecular weight samples in segment 2. This agrees well with many results described in the literature and can be explained with the model of Tadmor [17]. A decrease of the skin-layer thickness along the flow path has also been found by Altendorfer and Seitl [2]. Plessmann *et al.* [18] calculated the skin-layer thickness and reported a profile with a maximum near the injection gate and a decrease of the thickness proportional to the distance from the gate. Samples with a weld line show a steeper decrease of the skin-layer thickness from either gate to the centre of the mould. This has been explained by Altendorfer and Seitl [2] through a reduced flow-front velocity under constant temperature differences between melt and mould. A slower flow front causes a thicker skin layer. As we see (Table I) the molecular weight is of great influence. Comparing the samples with and without weld lines, we obtain for segment 1 and for $T_w = 40\,°C$ for the high molecular weight sample, skin-layer thicknesses $d_{with} = 334\,\mu m$ and $d_{without} = 258\,\mu m$, and for the low molecular weight sample $d_{with} = 15\,\mu m$ and $d_{without} = 201\,\mu m$.

A plot of the shear stress, σ_s, which has been determined from the stress–strain curves, (Fig. 4a) and the crystallinity, X_c, (Fig. 4b) over the skin-layer thickness reveals interesting correlations. The weld-line samples show a lower shear stress, and σ_s decreases with increasing skin-layer thickness. This is a consequence of the lower shear stress of the skin-layer volume: i.e. for a skin-layer thickness of 200 μm, the skin-layer volume is about one-sixth of the total volume of the bar.

The crystallinity, X_c, increases nearly proportional to the skin-layer thickness. This agrees with results of Trotignon *et al.* [4] and of Pleßmann *et al.* [18], who found an increased crystallinity in the skin layer. X_c also varies along the flow path. This is a result of the shear forces causing oriented crystallization in the skin layer [18].

A spherulitic morphology can be seen under the polarization microscope in the transition zone (zone II) and in the core (zone III). In the (textured) zone II, a number of spherulites with negative birefringence can be seen. These spherulites are identified as "β-form" spherulites from DSC and WAXS curves. The fraction of the β-modification contributing to the total crystallinity ("β-crystallinity"), $X_{c\beta}$, can be determined from the thermograms by calculating the ratio of the areas of the endotherms at 147.1 °C (β-peak) and at 165.4 °C (α-peak) (see Fig. 5), and from the WAXS curves by calculating the ratio of the "β-peak", ((2 0 0) reflection) to the rest of the curve after separation of the amorphous scattering (halo). $X_{c\beta}$ amounts to 5% in zone II for the low molecular weight sample and

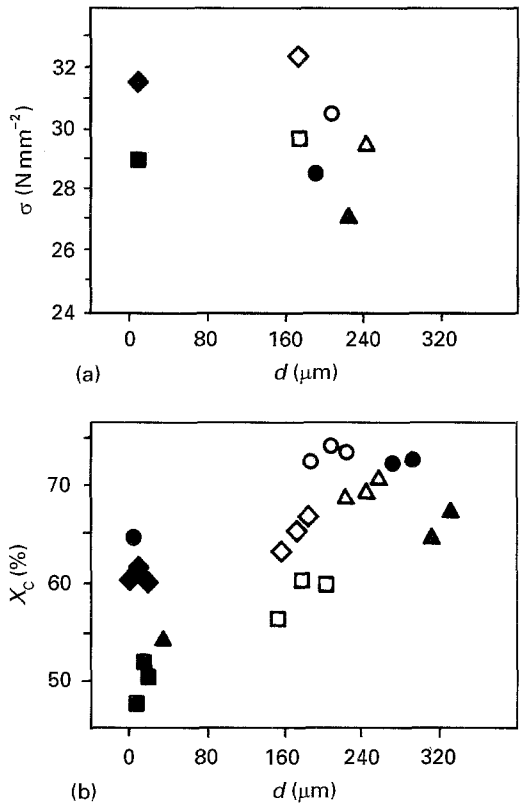

Figure 4 (a) Shear stress and (b) X-ray crystallinity as a function of skin-layer thickness: (□, ■) low molecular weight sample, $T_w = 40\,°C$; (◇, ◆) $T_w = 100\,°C$; (△, ▲) high molecular weight sample, $T_w = 40\,°C$; (○, ●) $T_w = 100\,°C$; (□, ◇, △, ○) without weld line, (■, ◆, ▲, ●) with weld line.

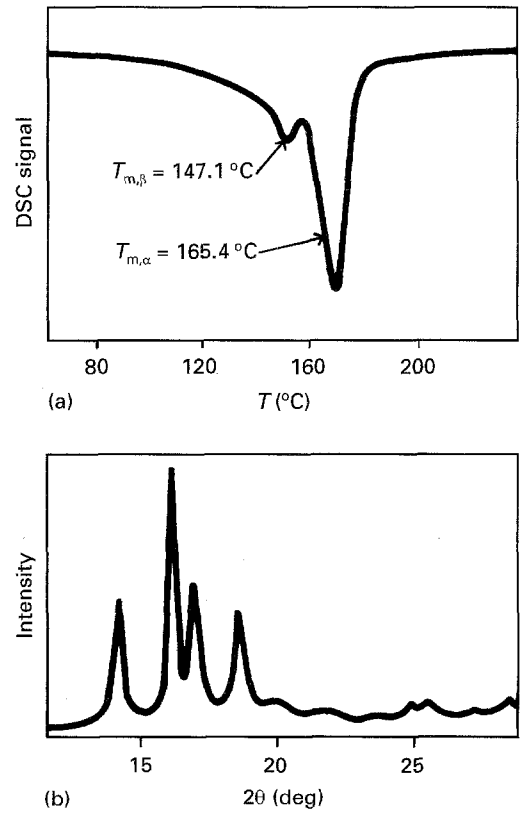

Figure 5 Identification of the β-modification: (a) DSC and (b) WAXS curves.

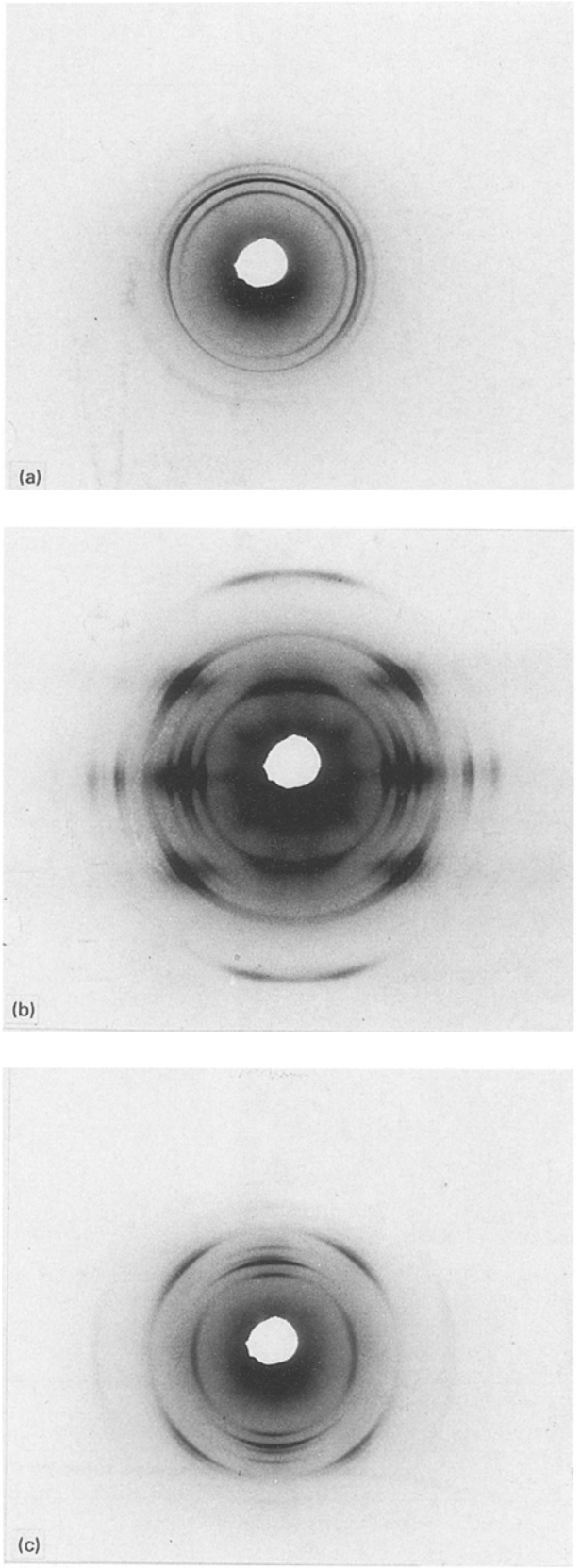

Figure 6 Flat-camera exposures taken from the skin layer of the high molecular weight sample, $T_w = 40\,°C$, segment 1 in (a) the *x*-direction (flow direction), (b) the *z*-direction, and (c) the *y*-direction (cf. Fig. 2).

11% for the high molecular weight sample. The core (zone II) shows no β-crystallinity. The β-crystallinity is higher for lower mould temperatures, and increases with molecular weight. Samples with weld line have a lower β-crystallinity, and in the weld line itself no

β-form spherulites occur [12]: at $T_w = 40\,°C$ the β-crystallinity is zero, at $T_w = 100\,°C$ it is below 2%.

Flat-camera exposures were taken from all microtomed sections. Fig. 6 shows the exposures taken from the skin layer of the high molecular weight sample at $T_w = 40\,°C$, segment 1 in flow direction (Fig. 6a) and in the two perpendicular directions (Fig. 6b and c). Two monoclinic modifications become visible, differing in orientation. The measured reflections are listed in Table II. One set of reflections is due to a unit cell whose *c*-axis is oriented parallel to the flow direction (*x*-direction in the figure), a second set of reflections ((1 1 0), (1 3 0) and (2 2 0) reflections) can be attributed to a unit cell with the *a**-axis parallel to the flow direction. The *a**-axis is oriented perpendicular to the *b*- and *c*-axes. This structure has been investigated by Clark and Spruiell [19] and by Fujiyama *et al.* [20]. Both groups found a bimodal orientation of the unit cell in both the skin layer and the core. In the skin layer, both *c*- and *a**-axes are oriented in the flow direction.

Orientation distribution functions can be calculated from the intensity distribution by using the equation

$$f(\theta) = \frac{1}{2}(3\overline{\cos^2\theta} - 1) = 1 - \frac{3}{2}\overline{\sin^2\theta} \qquad (1)$$

where θ is the angle between chain orientation and macroscopic orientation.

Calculating orientation functions for the *c*- (f_c), *b*- (f_b), and *a**- (f_{a^*}) axes, one finds f_c positive, f_b and f_{a^*} negative. An orientation in the flow direction, however, should give positive values for f_b and f_{a^*}. Fujiyama *et al.* [20] explained this as follows: when *c*-axis oriented and *a**-axis oriented components coexist, the *a**-axis of the *c*-axis oriented component and the *c*-axis of the *a**-axis oriented component are perpendicular to the flow direction. When calculating orientation functions, the *c*-axis of the *c*-axis oriented component and the *c*-axis of the *a**-axis oriented component contradict each other. The same holds for the *a**-axis with respect to the *c*- and *a**-axes orientations. If, as we find in the experiments, the orientation functions have different amounts, then the signs of the orientation functions f_c and f_{a^*} are determined by a balance of their absolute values and the degree of orientation of the *c*- and *a**-axis components. Therefore we find that the orientation of the *c*-axis component is higher than that of the *a**-axis component.

The orientation functions of the core have smaller values. The crystals in the core should therefore be unoriented. However, as the azimuthal intensity distribution of the (1 1 0) peaks show, f_c is positive. Therefore, also in the core, a *c*-axis orientation must exist [20, 21].

The orientation in the vicinity of the weld line can be estimated from the exposures shown in Fig. 7. From the analysis of the (0 4 0) reflection in Fig. 7a, a (weak) orientation of the *c*-axis parallel to the weld line is found. This orientation tilts by ~28° in Fig. 7b and c compared to Fig. 7a. We find the (1 1 0) and (2 2 0) reflections weak in the meridional direction and stronger in the equatorial direction (Fig. 7a–c), which indicates a uniaxial orientation of the unit cell. A small fraction of β-modification is measured (see Fig. 7a–c), which disappears at the surface of the segment (Fig. 7d). The (3 0 0) β-reflection in Fig. 7b and c tilts relative to the (*h k* 0) α-reflections by ~11°, due to the orientation of the β-crystals in the higher oriented transition zone.

Order parameters, *R*, for the α_1/α_2-transition have been determined from the areas under the (1 7 1), (1 3 2), (2 3 1), (0 5 1) reflections ($\alpha_1 + \alpha_2$ contributions) and the (2 4 1), (1 7 1) peaks (only α_2 contributions) [22–26]. The following typical values are obtained for rapidly cooled polypropylene: $R = 0.53$ in the skin and $R = 0.64$ in the core for $T_w = 40\,°C$ (segment 2) and for the low molecular weight sample. Injection from two gates does not change this value: for the sample with a weld line we found $R = 0.51$ in the skin and $R = 0.64$ in the core. For the high molecular weight sample, *R* amounts to 0.50 in the skin and 0.47 in the core. It is obvious that the type of injection is not responsible for the α_1/α_2-transition, but rather the cooling conditions in the mould. Awaya [27] found on similar samples, *R* values of 0.63 for rapidly cooled polypropylene and 0.62 for quenched (to 33 °C) samples. Annealing leads to *R* values of 2.02 (160 °C for 55 h) and 2.03 (155 °C for 29 h), and isothermal crystallization gives $R = 1.98$ (155 °C for 55 h). Therefore it can be understood why *R* increases only slightly with the distance from the gate (from 0.53 to 0.60 for the skin of the sample injected through one gate at $T_w = 40\,°C$) but more obviously with the melt temperature (from 0.53 (40 °C) to 0.79 (100 °C) for the same sample). The high molecular weight samples show slightly higher values. No difference is seen between samples with and without a weld line.

TABLE II Reflections measured from flat-camera exposures (ω = angle between equator and reflection, *D* = diameter of Debye reflections)

Peak	Peak position	ω(deg)	*D*(mm)	2θ(deg)	*d*(nm)	*h k l*	d_{lit}(nm)
1	Equat.	0	25	14.0	0.63	1 1 0	0.624
	Merid.	77.5	25	14.0	0.63	1 1 0	0.624
2(β)	Equat.	0	29	16.2	0.55	3 0 0	0.551
3	Equat.	0	30.5	17.0	0.52	0 4 0	0.52
4	Equat.	0	33.5	18.5	0.48	1 3 0	0.476
	Diag.	47	33.5	18.5	0.48	1 3 0	0.476
5	Diag.	41	38.5	21.1	0.42	1 1 1	0.416
6	Diag.	39	40.5	22.0	0.40	1 3 $\bar{1}$	0.406
7	Equat.	0	47.5	25.4	0.35	0 6 0	0.346
8	Equat.	0	55.5	28.8	0.30	2 2 0	0.312
	Merid.	77.5	55.5	28.8	0.30	2 2 0	0.312

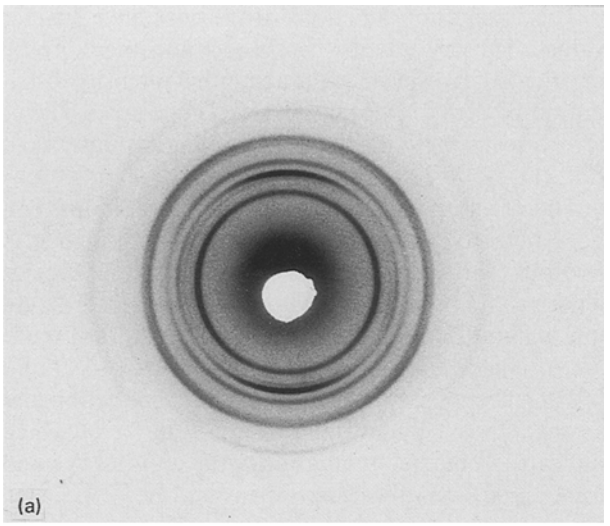

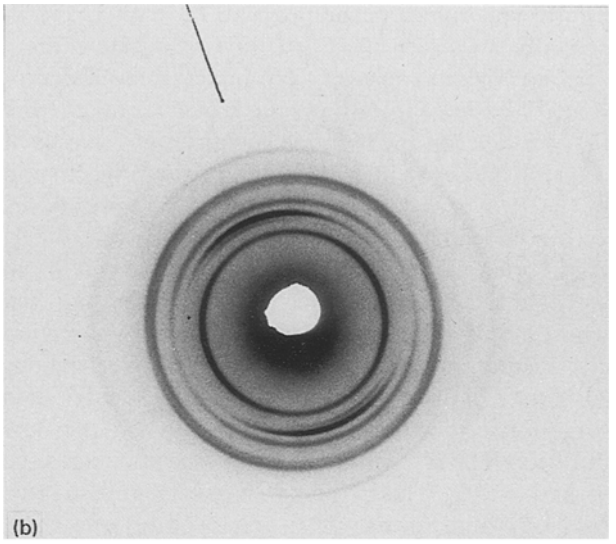

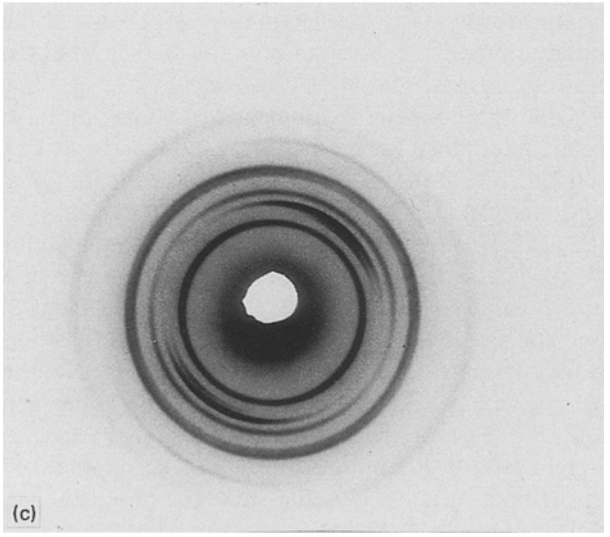

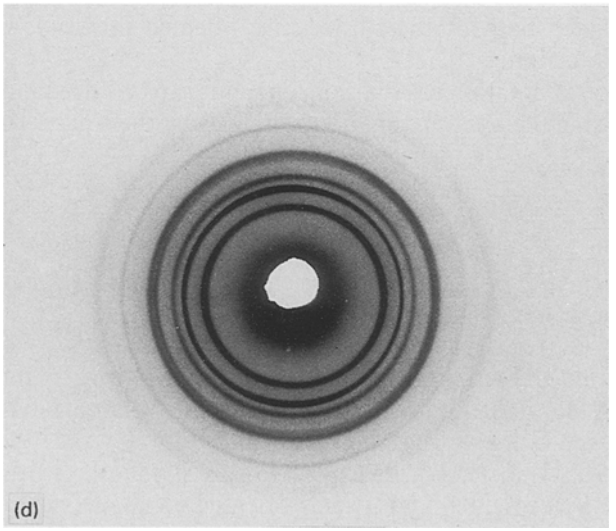

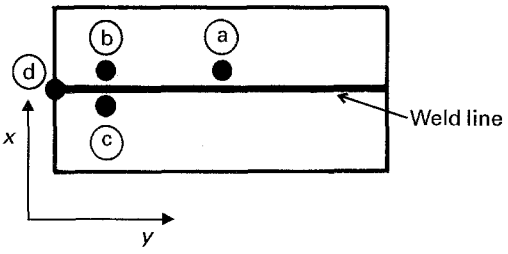

(e)

Figure 7 Orientation in the vicinity of the weld line (high molecular weight sample, $T_w = 100\,°C$, segment 2, skin layer), X-ray beam in the z-direction.

4. Conclusions

1. The skin-layer thickness depends on the molecular weight and on the type of injection: with increasing molecular weight, the skin-layer thickness increases, but in the vicinity of the weld line the skin layer almost disappears. This is due to the absence of longitudinal flow in the weld-line region and proves that, in this part of the sample, no crystallization in a stretched melt can take place. In agreement with the literature we find that the skin-layer thickness varies along the flow path of the melt and decreases with increasing mould temperature.

2. Several crystal modifications are found in the samples. While the core generally crystallizes in the monoclinic α-modification, the skin exhibits a considerable amount of β-modification. This modification can be traced not only in the textured outer skin, but also in the already spherulitic transition zone near the core. The fraction of β-modification depends on the mould temperature and on the molecular weight and amounts to 11% for the high molecular weight sample. In samples with weld lines, no β-crystallinity can be measured in the weld line. This demonstrates that, again, the shear of the melt induces β-type crystallization.

3. In the skin, a bimodal crystal orientation is found in agreement with earlier findings of Clark and Spruiell [19] and Fujiyama *et al.* [20] which almost disappears in the core. However, a weak c-axis orientation can be measured also in the core. In samples with a weld line, only c-axis orientation is found in the vicinity of the weld line, which correlates with the lower shear in the weld line.

4. The metastable α_1-modification is found in the skin layer. The values of the fraction of this modification to the stable α_2-modification coincide with expected values for rapid cooling of a polypropylene melt. The order parameter therefore depends only on

the cooling conditions of the melt. This proves that the formation of β-crystals is only a consequence of the shear forces in the stretched melt during injection.

References

1. M. R. KÀNTZ, F. H. NEWMAN and J. STIGALE, *J. Appl. Polym. Sci.* **16** (1972) 1249.
2. F. ALTENDORFER and E. SEITL, *Kunststoffe* **76** (1986) 47.
3. G. MENGES, G. WÜBKEN and B. HORN, *Colloid Polym. Sci.* **254** (1986) 267.
4. J. P. TROTIGNON, J. L. LEBRUN and J. VERDU, *Plast. Rubber Proc. Appl.* **2** (1982) 247.
5. E. FLEISCHMANN, P. ZIPPER, A. JANOSI, W. GEYMAYER, J. KOPPELMANN and J. SCHURZ, *Polym. Eng. Sci.* **29** (1989) 835.
6. H. JANESCHITZ-KRIEGL, *Rheol. Acta* **16** (1979) 327.
7. *Idem, ibid.* **18** (1979) 693.
8. B. FISA, *Polym. Compos.* **8** (1987) 408.
9. S. PICCAROLO and M. SAIU, *Plast. Rubber Proc. Appl.* **10** (1988) 11.
10. S. PICCAROLO, A. RALLIS and G. TITOMANLIO, *Int. Polym. Proc. II* **3** (1988) 137.
11. D. SINGH, H. G. MOSLE, M. KUNZ and W. WENIG, *J. Mater. Sci.* **25** (1990) 4704.
12. W. WENIG, D. SINGH, G. BOTZEN and H. G. MOSLE, *Angew. Makromol. Chem.* **179** (1990) 35.
13. Z. MENCIK, *J. Macromol. Sci. Phys.* **6** (1972) 101.
14. L. G. BERRY (ed.), Powder Diffraction File (JCPDS, Philadelphia, PA 1974).
15. G. WÜBKEN, Dissertation, RWTH Aachen (1974).
16. H. DRAGAUN, *Progr. Colloid Polym. Sci.* **62** (1977) 59.
17. Z. TADMOR, *J. Appl. Polym. Sci.* **18** (1974) 1753.
18. K. PLEßMANN, G. MENGES, M. CREMER, M. FENSKE, W. FESER, C. NETZE, H. OFFERGELD, G. PÖTSCH and H. STABREY, *Kunststoffe* **80** (1990) 200.
19. E. S. CLARK, J. E. SPRUIELL, *Polym. Eng. Sci.* **16** (1976) 176.
20. M. FUJIYAMA, T. WAKINO and Y. KAWASAKI, *J. Appl. Polym. Sci.* **35** (1988) 29.
21. A. SAKTHIVEL and A. S. ABHIRAMAN, *ibid.* **29** (1984) 4257.
22. P. CORRADINI, V. PETRACCONE and B. PIROZZI, *Eur. Polym. J.* **19** (1983) 299.
23. G. GUERRA, V. PETRACCONE, P. CORRADINI, C. DE ROSA and R. NAPOLITANO, *J. Polym. Sci. Polym. Phys. Ed* **22** (1984) 1029.
24. C. DE ROSA, G. GUERRA, R. NAPOLITANO, V. PETRACCONE and B. PIROZZI, *Eur. Polym. J.* **20** (1984) 937.
25. C. DE ROSA, G. GUERRA, R. NAPOLITANO, V. PETRACCONE and B. PIROZZI, *J. Therm. Anal.* **30** (1985) 1331.
26. R. NAPOLITANO, B. PIROZZI and V. VARRIALE, *J. Polym. Sci. Polym. Phys.* **28** (1990) 139.
27. H. AWAYA, *Polymer* **29** (1988) 591.

Received 22 December 1993
and accepted 16 August 1994